Theory and Processes of Formation and Sintering of Powder Materials
Теория и процессы формования и спекания порошковых материалов

UDC 536.425 + 621.762
https://doi.org/10.17073/1997-308X-2023-2-5-13

Research article
Научная статья

The impact of impurities on the Al–Fe–C system phase composition changes during sintering

E. N. Korosteleva, A. G. Knyazeva, M. A. Anisimova, I. O. Nikolaev

Institute of Strength Physics and Materials Science of the Siberian Branch of the Russian Academy of Sciences
2/4 Akademicheskii Prosp., Tomsk 634055, Russia

anna-knyazeva@mail.ru

Abstract. Manufacturing waste can be not only recycled but also utilized as a source of chemical elements and as a component of powder materials. Steel swarf are a complex multicomponent material with a high iron content, while impurities such as carbon can affect the diffusion interaction in the chip and metal powder mixture. In this study, we investigate the diffusion interaction between aluminum and steel swarf using temperature-controlled vacuum sintering. We analyzed the resulting mixture's microstructure and phase composition, and observed that sintering creates a multiphase structure in which FeAl iron aluminide occupies at least 30 vol. %. Despite the high sintering temperature, we also observed residual aluminum and iron. Incomplete transformation may result form refractory products that inhibit diffusion or impurities that influence the magnitude and direction of the diffusion fluxes. To confirm the impurities' role in the diffusion interaction kinetics, we developed simulation models of the intermetallic phase growth for a flat and spherical particle embedded in aluminum. The model consider cross-diffusion fluxes in the emerging phase regions and possible effects of impurities on the concentration limit for the new phase's existence. We derived approximate analytical solutions to analyze the emerging phase growth trends under various model parameters.

Keywords: metal swarf, reaction sintering, diffusion interaction, intermetallide phase, tests, simulation

Acknowledgements: This study is supported by the Russian Science Foundation and the Tomsk Oblast Administration, Grant No. 22-13-20031, https://rscf.ru/project/22-13-20031/

For citation: Korosteleva E.N., Knyazeva A.G., Anisimova M.A., Nikolaev I.O. The impact of impurities on the Al–Fe–C system phase composition changes during sintering. *Powder Metallurgy and Functional Coatings*. 2023;17(2):5–13. https://doi.org/10.17073/1997-308X-2023-2-5-13

Роль примесей в изменении фазового состава в системе Al–Fe–C при спекании

Е. Н. Коростелева, А. Г. Князева, М. А. Анисимова, И. О. Николаев

Институт физики прочности и материаловедения Сибирского отделения РАН
Россия, 634055, г. Томск, Академический пр-т, 2/46

anna-knyazeva@mail.ru

Аннотация. Эффективное использование материальных ресурсов заставляет активнее обращать внимание на отходы производства с целью не только простой их утилизации, но и их использования в качестве источника некоторых элементов и как компонентов порошковых материалов. Стальная стружка – сложный многокомпонентный материал на основе железа. Наличие примеси, например углерода, может оказывать влияние на диффузионное взаимодействие смеси стружки с порошком другого металла. В данной работе рассмотрен один из возможных

вариантов диффузионного взаимодействия алюминия и стальной стружки в условиях вакуумного спекания с регулируемым нагревом. После спекания был проведен микроанализ структуры и определен фазовый состав продуктов взаимодействия. Выявлено, что в процессе спекания формируется многофазная структура, в которой не менее 30 % объема занимает алюминид железа FeAl. Несмотря на достаточно высокие температуры, фиксируются остатки алюминия и железа. Среди причин неполного превращения могут быть тугоплавкие продукты взаимодействия, тормозящие диффузию, а также примеси, влияющие на величину и направленность диффузионных потоков. Для подтверждения важной роли примесей в кинетике диффузионного взаимодействия рассмотрены модельные задачи роста интерметаллидной фазы между частицей плоской или сферической формы с окружающим ее алюминием. Учитывается появление перекрестных диффузионных потоков в области растущей фазы и, возможно, влияние примеси на концентрационный предел существования новой фазы. Найдены приближенные аналитические решения, которые позволяют проанализировать динамику роста области, занимаемой растущей фазой, в зависимости от параметров модели.

Ключевые слова: металлическая стружка, реакционное спекание, диффузионное взаимодействие, интерметаллидная фаза, эксперимент, моделирование

Благодарности: Исследование выполнено при финансовой поддержке Российского научного фонда и субсидии администрации Томской области, грант № 22-13-20031, https://rscf.ru/project/22-13-20031/

Для цитирования: Коростелева Е.Н., Князева А.Г., Анисимова М.А., Николаев И.О. Роль примесей в изменении фазового состава в системе Al–Fe–C при спекании. *Известия вузов. Порошковая металлургия и функциональные покрытия*. 2023;17(2):5–13. https://doi.org/10.17073/1997-308X-2023-2-5-13

Introduction

Steels and other iron alloys remain the most widely used and cost-effective material in the manufacturing industry. Materials scientists design new and more efficient materials to replace conventional alloys, while also seeking ways to recycle and reuse retired products, components, and waste [1–4]. The largest source of manufacturing waste is generated by machining, which produces metal swarf [5; 6]. It should be noted that steel swarf are complex, multicomponent materials containing iron and carbon [7].

The swarf may also contain other alloying elements in varying concentrations. For example, lowest steel grades (e.g., steel 45 [ANSI analog: 1045]) contain 0.42 to 0.5 wt. % of carbon. Other most significant alloying elements are manganese (up to 0.8 %) and silicon (up to 0.37 %). The steel specification allows for the presence of chromium, copper, and nickel (up to 0.3 % each), as well as a low amount of phosphorus and sulfur (up to 0.035 %). Steel swarf are formed by the high-speed cutting of the metal workpiece resulting in an activated, highly defective structure of the chip surface [8].

Swarf are typically remelted, following cleaning to remove oxidation products and coolant [9], and then compacted into briquettes. However, steel swarf can be used as a component of powder mixtures with other elements [10]. Given that fragmented steel swarf contain multiple elements, understanding their diffusion interaction with other components of the mixture under heating is of interest. a better understanding of this process will contribute to the development of new materials and metal waste recycling technologies.

The objective of this study is to analyze the effects of impurities on the diffusion interaction between the components of the Al–Fe–C system.

Materials and methods

Aluminum was used as the primary component of our mixture, which interacted with fragmented steel swarf. The Al–Fe system has been extensively studied [11–16], and aluminum is utilized both as a matrix and as an alloying element. The Al–Fe phase diagram [17] reveals that aluminum has high solubility in α-Fe, forming large areas of solid solutions (up to 32 at. %). Its solubility in γ-Fe drops to 1.285 at. % at high temperatures. The solubility of iron in aluminum is very low, with a maximum of 0.03 at. % at the 654 °C eutectic temperature. The system produces five stable intermetallic compounds (Fe_3Al, FeAl, $FeAl_2$, Fe_2Al_5 и $FeAl_3$) and their temperature range for existence is 552 to 1170 °C.

We studied a mixture of fragmented steel swarf (75 wt. %) created by machining a steel 45 grade workpiece and the PA-4 aluminum powder (25 wt. %). The mixture was heated to 1000 °C in a vacuum furnace, and the phase composition of the powder was examined by analyzing the microstructure after sintering.

Figure 1 displays the surface of a steel chip fragment and its microstructure after sintering. Our analysis indicated that the carbon component concentration did not exceed 1.5 %. Jäger S. et al. [18] conducted a detailed investigation of steel chip sintering.

As aluminum was added to the steel swarf, intermetallic compound s were synthesized, resulting in a multiphase structure (Figure 2) in which at least 30 vol. % is occupied by the FeAl iron aluminide. Despite the exothermic nature of the Al and Fe interaction, residual Al (at least 15 vol. %), and Fe were discovered by XRD in the vacuum sintering products. This indicate that the reactions between Al and Fe (the base element of the steel 45 grade swarf) were not completed even at the sintering temperature of 1000 °C when Al was in liquid state.

In the contact area between interacting particles where diffusion interaction occurs, there are various factors that can affect the flux dynamics and completeness of phase transformations. These factors may include:

– refractory interaction products that inhibit diffusion;

– impurities that affect the magnitude and direction of the diffusion fluxes;

– structural imperfections that affect diffusion and reactions at the micro level.

Although the impurities may not directly contribute to the formation of new phases, they can significantly impact the kinetics of phase formation.

In order to confirm the impact of the impurities, we proposed a simulation model.

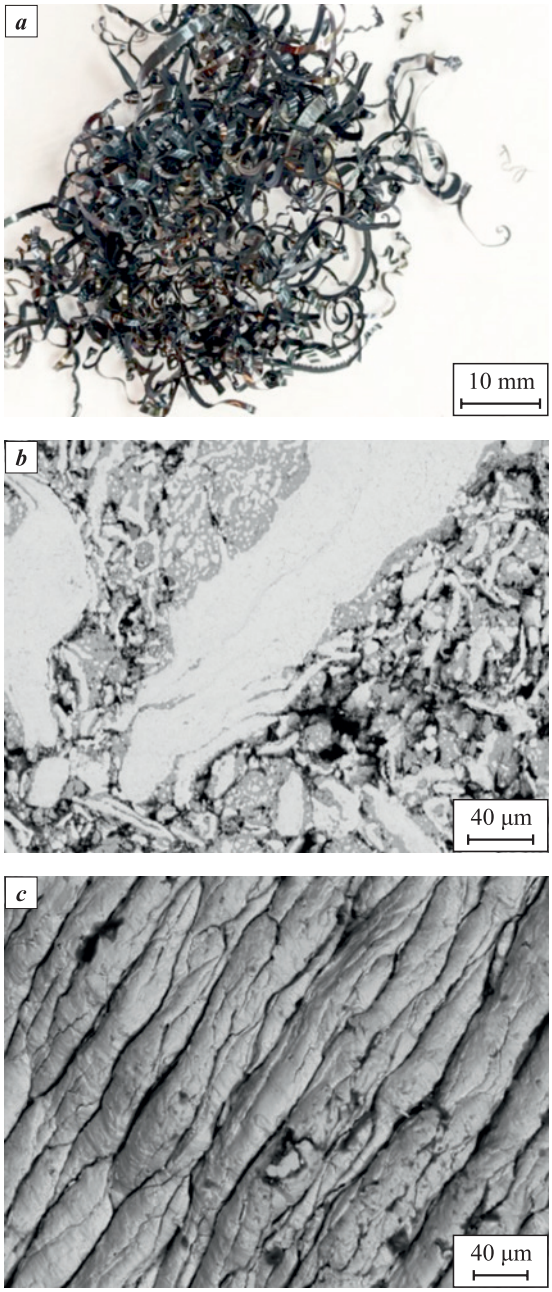

Fig. 1. Appearance (***a***) and surface morphology (***b***) of the steel 45 grade swarf. Chip microstructure after fragmenting and sintering at 1000 °C (***c***)

Рис. 1. Общий вид (***a***) и морфология поверхности (***b***) стальной стружки из стали 45, а также ее микроструктура после измельчения и спекания при 1000 °C (***c***)

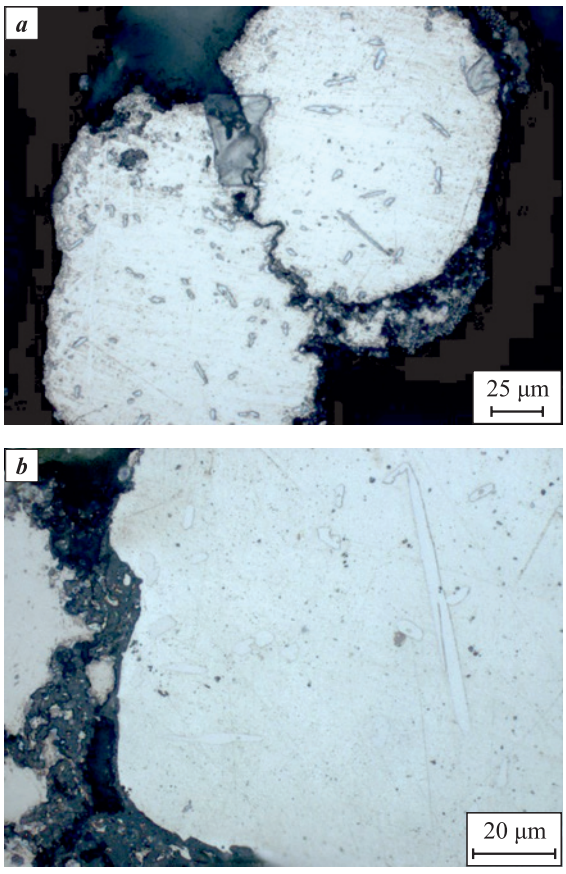

Fig. 2. Microstructure of the synthesized powders (25 % Al + 75 % steel 45)
a – appearance, ***b*** – intraparticle distribution of iron aluminide needle-like grains

Рис. 2. Микроструктура синтезированных порошковых продуктов состава 25 % Al + 75 % сталь 45
a – общий вид, ***b*** – внутричастичное распределение зерен-игл из алюминидов железа

Simulation model

The problem statement assumes that iron, as the primry component of the steel ships, has low solubility in Al. However, the solubility of aluminum in iron,although also limited, should be considered, with a value of 1.285 % at $t = 1150$ °C, which is the high-temperature solubility in γ-Fe. It is also assumed that each phase contains an area of homogeneity. Additionally, the steel swarf obtained by machining steel workpieces contain carbon as an impurity, with a maximum content of 1.5 %, accounting for possible contamination. It should be noted that the model for Fe and Al diffusion interaction in the presence of a third component can vary depending on the known diffusion path variations and higher phase competition in systems with more than two components [19; 20]. Cross-diffusion fluxes can result in an irregular concentration distribution in such systems [21–23].

1. The first version of the proposed model assumes a flat body for the chip, as shown in Fig. 1, *a*. Aluminum reacts with the iron at the surface, leading to the formation of intermetallic phases. Carbon influences diffusion by facilitating cross-diffusion fluxes. At any given moment, each phase may contain Fe, C, and Al. The model incorporates two moving boundaries, separating three regions that contain the three phases: (Fe + C)–(Fe_xAl_y)–(Al) (Figure 3). The intermetallic phases are located between the moving boundaries.

The sum of the three mass concentrations in each phase is always equal to 1 at any given point. Typically, two diffusion equations for each region are abequate:

$$\frac{\partial C_{1,k}}{\partial t} = \frac{\partial}{\partial x}\left(D_{11}^{(k)} \frac{\partial C_{1,k}}{\partial x} \right) + \frac{\partial}{\partial x}\left(D_{12}^{(k)} \frac{\partial C_{2,k}}{\partial x} \right), \qquad (1)$$

$$\frac{\partial C_{2,k}}{\partial t} = \frac{\partial}{\partial x}\left(D_{21}^{(k)} \frac{\partial C_{1,k}}{\partial x} \right) + \frac{\partial}{\partial x}\left(D_{22}^{(k)} \frac{\partial C_{2,k}}{\partial x} \right), \qquad (2)$$

where the k superscript can be p, ph, m and represent the Fe + C, Fe_xAl_y and Al(C, Fe) regions; $C_{1,k}$ is the iron concentration; $C_{2,k}$ is the carbon concentration in each region; $D_{ij}^{(k)}$ are the partial diffusion coefficients.

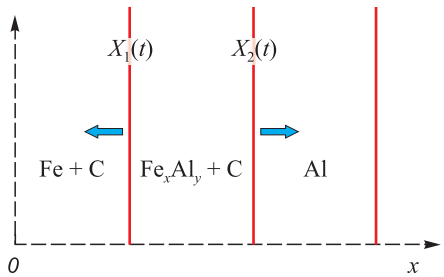

Fig. 3. Phase regions and moving boundaries

Рис. 3. Иллюстрация к математической постановке задачи

The symmetry condition is fulfilled at the center of the particle:

$$x = 0 : \frac{\partial C_{1,p}}{\partial x} = 0; \quad \frac{\partial C_{2,p}}{\partial x} = 0. \qquad (3)$$

The conditions at the phase interfaces are as follows:

$$\begin{gathered} x = x_1(t) : C_{1,p} = C_{10}, \; C_{2,p} = C_{20}, \; C_{1,ph} = \varphi_1, \\ C_{2,ph} = \gamma_1 C_{2,p} \equiv \gamma_1 C_{20}, \\ \left(C_{1,p} - C_{1,ph}\right)\frac{dx_1}{dt} = -J_{1,ph} \quad \text{or} \quad \left(C_{10} - \varphi_1\right)\frac{dx_1}{dt} = -J_{1,ph}, \end{gathered} \qquad (4)$$

where C_{10}, C_{20} are the initial concentrations of iron and carbon, respectively, in the mixture particles; φ_1 is the iron solubility limit in the transition region containing Fe_3Al;

$$\begin{gathered} x = x_2(t) : C_{1,ph} = \varphi_2, \; C_{1,m} = 0, \\ \left(C_{1,ph} - C_{1,m}\right)\frac{dx_2}{dt} = J_{1,ph} \quad \text{or} \quad \varphi_2 \frac{dx_2}{dt} = J_{1,ph}, \end{gathered} \qquad (5)$$

$$-D_{21}\frac{\partial C_{1,ph}}{\partial x} - D_{22}\frac{\partial C_{2,ph}}{\partial x} = -D_m \frac{\partial C_{2,m}}{\partial x}, \qquad (6)$$

$$C_{2,ph}\gamma_2 = C_{2,m}, \qquad (7)$$

where φ_2 is the iron solubility limit in the transition region containing $FeAl_3$. It depends on the carbon concentration as follows:

$$\varphi_2 = \varphi_{20}\left(1 - \beta C_{2,ph}\right).$$

The impermeability condition applies to the outer boundary:

$$x = R_m : \frac{\partial C_{2,m}}{\partial x} = 0. \qquad (8)$$

The equations for the diffusion fluxes in the region where a new phase emerges are given below

$$J_{1,ph} = -D_{11}\frac{\partial C_{1,ph}}{\partial x} - D_{12}\frac{\partial C_{2,ph}}{\partial x}, \qquad (9)$$

$$J_{2,ph} = -D_{21}\frac{\partial C_{1,ph}}{\partial x} - D_{22}\frac{\partial C_{2,ph}}{\partial x}. \qquad (10)$$

At the initial moment

$$\begin{gathered} t = 0 : C_{1,p} = C_{1,p0} = 0.995, \; C_{2,p} = C_{2,p0} = 0.005, \\ C_{1,m} = 0, \; C_{2,m} = 0, \; C_{1,ph} = 0, \; C_{2,ph} = 0, \\ x_1 = x_{10} = R_0, \; x_2 = x_{20} = R_0. \end{gathered}$$

Assuming the low solubility of aluminum in iron and iron in aluminum, we made an assumption that the concentrations of iron and carbon are constant in the Fe + C region i.e., to the left of the moving boundary $X_1(t)$, and only carbon is allowed to diffuse into the Al region to the right of $X_2(t)$. Therefore, the concentrations to the left of the $X_1(t)$ moving boundary can be expressed as

$$C_{1,p} = C_{1,p0},\ C_{2,p} = C_{2,p0}, \tag{11}$$

and to the right of $X_2(t)$

$$\frac{\partial C_{2,m}}{\partial t} = D_m \frac{\partial^2 C_{2,m}}{\partial x^2}. \tag{12}$$

Hereinafter, we omit the k superscript at the diffusion coefficients of the emerging phase.

To obtain an analytical solution, we used the quasi-static approximation and assume for equations (1), (2) and (12)

$$\frac{\partial C_{1,ph}}{\partial t} = 0,\ \frac{\partial C_{2,ph}}{\partial t} = 0,\ \frac{\partial C_{2,m}}{\partial t} = 0.$$

Then Eq. (1) and (2) take the form

$$\frac{d}{dx}\left(D_{11}\frac{dC_{1,ph}}{dx}\right) + \frac{d}{dx}\left(D_{12}\frac{dC_{2,ph}}{dx}\right) = 0,$$

$$\frac{d}{dx}\left(D_{21}\frac{dC_{1,ph}}{dx}\right) + \frac{d}{dx}\left(D_{22}\frac{dC_{2,ph}}{dx}\right) = 0.$$

These equations are equivalent to the following:

$$\frac{d}{dx}\left(\frac{dC_{1,ph}}{dx}\right) = 0,\ \frac{d}{dx}\left(\frac{dC_{2,ph}}{dx}\right) = 0.$$

The solution is

$$C_{1,ph}(x) = A_1 x + B_1 \text{ и } C_{2,ph}(x) = A_2 x + B_2, \tag{13}$$

where A_1, A_2, B_1, B_2 are the integration constants.

By substituting Eq. (13) into the concentration boundary conditions, we obtained the following system of linear algebraic equations:

$$x = x_1(t) : \varphi_1 = A_1 x_1 + B_1,\ \gamma_1 C_{20} = A_2 x_1 + B_2, \tag{14}$$

$$x = x_2(t) : \left(\varphi_{20} - \varphi_{20}\beta_2\left[A_2 x_2 + B_2\right]\right) = A_1 x_2 + B_1, \tag{15}$$

$$D_{21}A_1 + D_{22}A_2 = 0. \tag{16}$$

The solution is:

$$A_1 = D_{22}\alpha\frac{1}{x_2 - x_1},\ B_1 = \varphi_1 - D_{22}\alpha\frac{x_1}{x_2 - x_1},$$

$$A_2 = -D_{21}\alpha\frac{1}{x_2 - x_1},\ B_2 = \gamma_1 C_{20} + D_{21}\alpha\frac{x_1}{x_2 - x_1},$$

where

$$\alpha = \frac{\varphi_1 - \varphi_{20}\left(1 - \beta\gamma_1 C_{20}\right)}{\varphi_{20}\beta D_{21} + D_{22}}. \tag{17}$$

Then flux equation (9) is

$$J_{1,ph} = -D_{11}A_1 - D_{12}A_2 = -\frac{\alpha\Delta}{x_2 - x_1}, \tag{18}$$

where $\Delta = D_{11}D_{22} - D_{12}D_{21}$.

Then we found the equations for the moving boundaries from diffusion flux conditions (4) and (5):

$$\begin{gathered}\left(C_{10} - \varphi_1\right)\frac{dx_1}{dt} = \frac{\alpha\Delta}{x_2 - x_1}, \\ \varphi_{20}\left(1 - \beta C_{2,ph}\right)\frac{dx_2}{dt} = -\frac{\alpha\Delta}{x_2 - x_1}.\end{gathered} \tag{19}$$

By substituting the integration constant expressions into (13), we obtained $C_{2,ph}$:

$$C_{2,ph}(x_2) = -D_{21}\alpha\frac{1}{x_2 - x_1}x_2 + \gamma_1 C_{20} +$$

$$+ D_{21}\alpha\frac{x_1}{x_2 - x_1} = \gamma_1 C_{20} - D_{21}\alpha.$$

It follows that

$$\varphi_{20}\left(1 - \beta\left[\gamma_1 C_{20} - D_{21}\alpha\right]\right)\frac{dx_2}{dt} = -\frac{\alpha\Delta}{x_2 - x_1}. \tag{20}$$

It follows from (19) and (20) that

$$\chi\frac{dx_1}{dx_2} = -1,$$

where $\chi = \dfrac{C_{10} - \varphi_1}{\varphi_{20}\left(1 - \beta\left[\gamma_1 C_{20} - D_{21}\alpha\right]\right)}$, therefore

$$x_2 = -\chi x_1 + F'. \tag{21}$$

At the initial moment, both boundaries are at R_0:

$$R_0 = -\chi R_0 + F',$$

then

$$F' = R_0(1 + \chi),\ x_2 = -\chi x_1 + R_0(1 + \chi),$$

$$\left(C_{10} - \varphi_1\right)\frac{dx_1}{dt} = \frac{\alpha\Delta}{\left(R_0 - x_1\right)\left(\chi + 1\right)}.$$

Therefore the equation for the x_1 boundary is

$$\frac{(x_1 - R_0)^2}{2} = -\frac{\alpha \Delta t}{(C_{10} - \varphi_1)(1+\chi)} + F'', \qquad (22)$$

where F'' is the integration constant. It follows from the initial conditions that $F'' = 0$.

The positions of the boundaries are governed by the parabolic law and are influenced by the cross-diffusion fluxes. These velocities vary due to the modifications in the homogeneity region of the intermetallic phase, as illustrated in Figure 4. It shows the boundary positions vs. time curves (top curves: x_2 boundary; bottom curves: x_1 boundary).

We assumed the following: $D_{11} = 3.63 \cdot 10^{-10}$, $D_{12} = 2.47 \cdot 10^{-12}$, $D_{22} = 3.32 \cdot 10^{-11}$, $D_{21} = 1.84 \cdot 10^{-12}$ m^2/s, $R_0 = 100$ μm.

Note that if there are cross fluxes only, it follows from (22) that

$$\frac{(x_1 - R_0)^2}{2} = -\frac{\varphi_1 - \varphi_{20}}{D_{22}} \varphi_{20} \frac{D_{11}D_{22} - D_{12}D_{21}}{(C_{10} - \varphi_1)(C_{10} - \varphi_1 + \varphi_{20})} t,$$

and if there are no impurities, then

$$\frac{(x_1 - R_0)^2}{2} = -\frac{D_{11}(\varphi_1 - \varphi_{20})\varphi_{20} t}{(C_{10} - \varphi_1)(C_{10} - \varphi_1 + \varphi_{20})}.$$

The presence of cross-diffusion fluxes can lead to both acceleration and deceleration of the boundary movement (faster or slower phase formation) depending on the sign of the $D_{12}D_{21}$ product. The expansion of the phase homogeneity region is always unidirectional. It means that the first option ($D_{12}D_{21} > 0$) is more likely observed in the tests.

If we consider the φ_1 vs. carbon concentration relationship, the solution is similar.

2. The second version of the model simulates spherical particles.

The diffusion equations for the transition layer in the spherical coordinate system take the form

$$\frac{\partial C_{1,ph}}{\partial t} = \frac{1}{r^2}\frac{\partial}{\partial r}\left(r^2 D_{11}\frac{\partial C_{1,ph}}{\partial r}\right) + \frac{1}{r^2}\frac{\partial}{\partial r}\left(r^2 D_{12}\frac{\partial C_{2,ph}}{\partial r}\right),$$

$$\frac{\partial C_{2,ph}}{\partial t} = \frac{1}{r^2}\frac{\partial}{\partial r}\left(r^2 D_{21}\frac{\partial C_{1,ph}}{\partial r}\right) + \frac{1}{r^2}\frac{\partial}{\partial r}\left(r^2 D_{22}\frac{\partial C_{2,ph}}{\partial r}\right),$$

where r is the radial coordinate.

A quasi-stationary approximation is

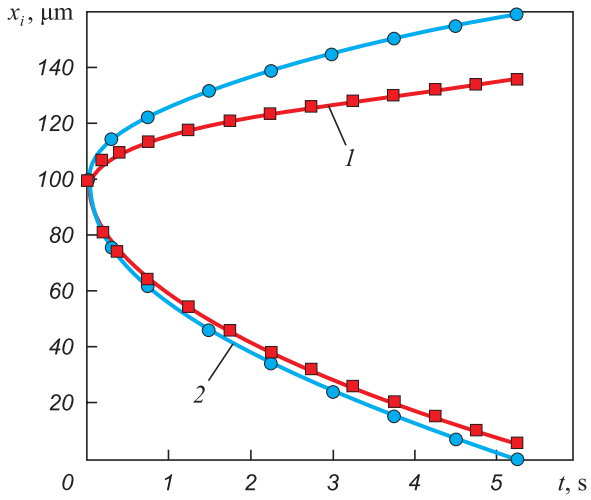

Fig. 4. Boundary positions vs. time curves (for flat particles)
1 – β = 1; ***2*** – β = 10 ($\gamma_1 = 1$)

Рис. 4. Положение границ в условиях плоской частицы
1 – β = 1; ***2*** – β = 10 ($\gamma_1 = 1$)

$$\frac{1}{r^2}\frac{d}{dr}\left(r^2 D_{11}\frac{dC_{1,ph}}{dr}\right) + \frac{1}{r^2}\frac{d}{dr}\left(r^2 D_{12}\frac{dC_{2,ph}}{dr}\right) = 0,$$

$$\frac{1}{r^2}\frac{d}{dr}\left(r^2 D_{21}\frac{dC_{1,ph}}{dr}\right) + \frac{1}{r^2}\frac{d}{dr}\left(r^2 D_{22}\frac{dC_{2,ph}}{dr}\right) = 0.$$

The boundary conditions and solution are similar to the previous case. The distribution of concentration is

$$C_{1,ph}(r) = -\frac{A_1}{r} + B_1, \; C_{2,ph}(r) = -\frac{A_2}{r} + B_2, \qquad (23)$$

where

$$A_1 = -\alpha D_{22}\frac{x_1 x_2}{x_1 - x_2}, \; B_1 = -\alpha D_{22}\frac{x_2}{x_1 - x_2} + \varphi_1,$$
$$A_2 = \alpha D_{21}\frac{x_1 x_2}{x_1 - x_2}, \; B_2 = \alpha D_{21}\frac{x_2}{x_1 - x_2} + \gamma_1 C_{20}. \qquad (24)$$

The expression for the flux is similar to (9). By accounting for solutions (23), (24), it takes the form

$$J_{1,ph} = -\left(D_{11}\frac{A_1}{r^2} + D_{12}\frac{A_2}{r^2}\right) =$$
$$= -\frac{1}{r^2}\alpha\frac{x_1 x_2}{x_1 - x_2}\left(-D_{11}D_{22} + D_{12}D_{21}\right) =$$
$$= \Delta\alpha\frac{x_1 x_2}{x_1 - x_2}\frac{1}{r^2}. \qquad (25)$$

Consequently, we derived the equation for moving boundaries and the boundary ratio from the conditions similar to (4) and (5):

$$\chi\frac{dx_1}{dx_2}=-\frac{x_2^2}{x_1^2} \text{ and } x_2=-\sqrt[3]{\chi}x_1+F',$$

where

$$F'=R_0\left(1+\sqrt[3]{\chi}\right),$$

$$\chi=\frac{C_{10}-\varphi_1}{\varphi_{20}\left(1-\beta\left[\gamma_1 C_{20}-D_{21}\alpha\right]\right)}.$$

We again came to the parabolic law. It differs from the previous one only by the impact of its variables:

$$\frac{\left(R_0-x_1\right)^2}{2}=-\frac{\alpha\Delta t}{\left(C_{10}-\varphi_1\right)\left(1+\sqrt[3]{\chi}\right)}.$$

Figure 5 shows the difference in interphase velocities for particles of different shapes.

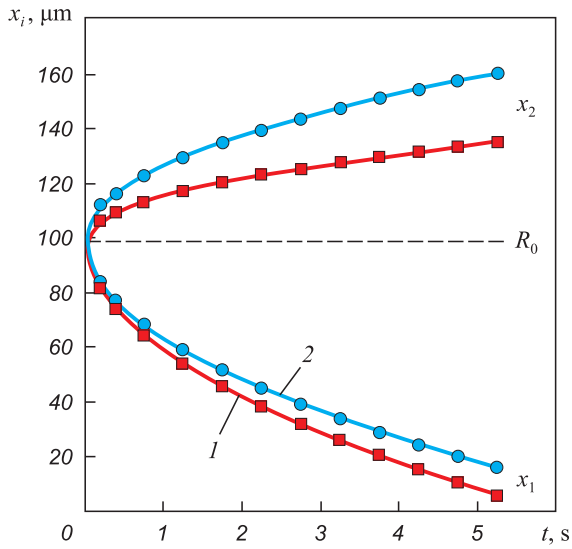

Fig. 5. Boundary position vs. time curves for flat (***1***) and spherical (***2***) particles. Assumptions: $\gamma_1 = 1$, $\beta = 1$, $\varphi_1 = 0.85$, $\varphi_{20} = 0.4$, $C_{10} = 0.995$, $C_{20} = 0.005$

Рис. 5. Изменение положения границ со временем для плоской (***1***) и сферической (***2***) частиц при следующих условиях: $\gamma_1 = 1$, $\beta = 1$, $\varphi_1 = 0{,}85$, $\varphi_{20} = 0{,}4$, $C_{10} = 0{,}995$, $C_{20} = 0{,}005$

Conclusions

The study revealed that the vacuum sintering of fragmented steel swarf with powdered aluminum does not achieve complete phase transformations, despite the exothermic nature of the intermetallic synthesis reaction. The initial phases were observed in the final product.

Our findings suggest that impurities in the swarf can affect the phase growth rate by inducing cross-diffusion fluxes and altering the size of the emerging phase homogeneity region. This effect was observed in both flat and spherical particles.

References / Список литературы

1. Rovin S.L., Kalinichenko A.S., Rovin L.E. The return of the dispersed metal waste into production. *Litiyo i metallurgiya*. 2019;(1):45–48. (In Russ.).
https://doi.org/10.21122/1683-6065-2019-1-45-48
Ровин С.Л., Калиниченко А.С., Ровин Л.Е. Возвращение дисперсных металлоотходов в производство. *Литье и металлургия*. 2019;(1):45–48.
https://doi.org/10.21122/1683-6065-2019-1-45-48
2. Chang J.I., Lin J.J., Huang J.S., Chang Y.M. Recycling oil and steel from grinding swarf. *Resources, Conservation and Recycling*. 2006;49(2):191–201.
https://doi.org/10.1016/j.resconrec.2006.03.014
3. Djakonov O.M. Production of metallurgical briquettes on the basis of chips-powder compositions by hot press molding. *Litiyo i metallurgiya*. 2011;(4):129–137. (In Russ.).
Дьяконов О.М. Получение металлургических брикетов на основе стружко-порошковых композиций горячим прессованием. *Литье и металлургия*. 2011;(4):129–137.
4. Andersson A., Gullberg A., Kullerstedt A., Sandberg E., Andersson M., Ahmed H., Sundqvist-Ökvist L., Björkman B. A holistic and experimentally-based view on recycling of off-gas dust within the integrated steel plant. *Metals*. 2018;8(10):760.
https://doi.org/10.3390/met8100760
5. Rovin S.L., Rovin L.E., Zayac T.M., Valickaya O.M. Recycling of ferrous metal shavings. *Litiyo i metallurgiya*. 2017;89(4):94–101. (In Russ.).
https://doi.org/10.21122/1683-6065-2017-4-94-101
Ровин С.Л., Ровин Л.Е., Заяц Т.М., Валицкая О.М. Переработка стружки черных металлов. *Литье и металлургия*. 2017;89(4):94–101.
https://doi.org/10.21122/1683-6065-2017-4-94-101
6. Hankel J., Jager S., Weber S. Development of a recycling strategy for grinding sludge using supersolidus liquid phase sintering. *Journal of Cleaner Production*. 2020;263:121501.
https://doi.org/10.1016/j.jclepro.2020.121501
7. Dyakonov O.M. Investigation of physicochemical and mechanical characteristics of steel and cast iron chips. *Litiyo i metallurgiya*. 2009;(4):161–173. (In Russ.).
Дьяконов О.М. Исследование физико-химических и механических свойств стальной и чугунной стружки. *Литье и металлургия*. 2009;(4):161–173.
8. Loginov Yu.N., Zagirov N.N., Ivanov E.V. Evaluation of the level of hardening of aluminum alloy chips intended for subsequent pressure treatment. *Obrabotka metallov (tekhnologiya, oborudovanie, instrumenty)*. 2021;23(1):45–55. (In Russ.).
Логинов Ю.Н., Загиров Н.Н., Иванов Е.В. Оценка уровня упрочнения стружки из алюминиевого сплава,

предназначенной для последующей обработки давлением. *Обработка металлов (технология, оборудование, инструменты)*. 2021;23(1):45–55.

9. Mahmooda K., Ul Haq Syed W., Pinkerton A.J. Innovative reconsolidation of carbon steel machining swarf by laser metal deposition. *Optics and Lasers in Engineering*. 2011;49(2):240–247. https://doi.org/10.1016/j.optlaseng.2010.09.014
10. Gnatko M., Li C., Arnold A., Freidrich B. Purification of aluminium cast alloy melts through precipitation of Fe-containing intermetallic compounds. *Metals*. 2018;8(10):796. https://doi.org/10.3390/met8100796
11. Shahid R.N., Scudino S. Strengthening of Al–Fe_3Al composites by the generation of harmonic structures. *Scientific Reports*. 2018;8:6484. https://doi.org/10.1038/s41598-018-24824-y
12. Tomida S., Nakata K. Fe–Al composite layers on aluminum alloy formed by laser surface alloying with iron powder. *Surface and Coatings Technology*. 2003;174-175:559–563. https://doi.org/10.1016/S0257-8972(03)00698-4
13. Minamino Y., Koizumi Y., Tsuji N., Hirohata N., Mizuuchi K., Ohkanda Y. Microstructures and mechanical properties of bulk nanocrystalline Fe–Al–C alloys made by mechanically alloying with subsequent spark plasma sintering. *Science and Technology of Advanced Materials*. 2004;5(1-2):133–143. https://doi.org/10.1016/j.stam.2003.11.004
14. Najafi A., Movahedi M., Yarandi A.S. Properties–microstructure relationship in Al–Fe in situ composite produced by friction stir processing. *Proceedings of the Institution of Mechanical Engineers, Part L: Journal of Materials: Design and Applications*. 2019;233(10):1955–1965. https://doi.org/10.1177/1464420718803752
15. Kopec M., Jóźwiak S., Kowalewski Z. Fe–Al based composite reinforced with ultra-fine Al_2O_3 oxides for high temperature applications. *Journal of Theoretical and Applied Mechanics*. 2021;59(3):509–513. https://doi.org/10.15632/jtam-pl/138322
16. Kostov A., Friedrich B., Zivković D. Thermodynamic calculations in alloys Ti–Al, Ti–Fe, Al–Fe and Ti–Al–Fe. *Journal of Mining and Metallurgy, Section B: Metallurgy*. 2008;44(1):49–61. https://doi.org/10.2298/JMMB0801049K
17. State Diagrams of Double Metal Systems: Handbook. In 3 vol. T. 1 / Ed. by N.P. Lyakishev. Moscow: Mashinostroenie, 1996. 991 p. (In Russ).

    Диаграммы состояния двойных металлических систем: справочник. В 3 т. Т. 1 / Под ред. Н.П. Лякишева. М: Машиностроение, 1996. 991 с.
18. Jäger S., Weber S. Upcycling strategy of grinding swarf by super solidus liquid phase sintering. *Procedia CIRP*. 2020;90:546–551. https://doi.org/10.1016/j.procir.2020.01.079
19. Wierzba B. Phase competition in ternary Ti–Ni–Al system. *Physica A: Statistical Mechanics and its Applications.* 2016;454:110–116. https://doi.org/10.1016/j.physa.2016.02.068
20. Ji Y., Abernathy H.W., Chen L.-Q. Thermodynamic models of multicomponent nonstoichiometric solution phases using internal process order parameters. *Acta Materialia*. 2022;223:117462. https://doi.org/10.1016/j.actamat.2021.117462
21. Knyazeva A.G. Difusion following the vacancy mechanism in materials with large number of internal surfaces. *Chemistry for Sustainable Development*. 2005;13(2): 233–242.
22. Belova I.V., Murch G.E. Analysis of interdiffusion data in multicomponent alloys to extract fundamental diffusion information. *Journal of Phase Equilibria and Diffusion*. 2006;27(6): 629–637. https://doi.org/10.1007/BF02736565
23. Svoboda J., Fischer F.D., Abart R. Modeling of diffusional phase transformation in multi-component systems with stoichiometric phases. *Acta Materialia*. 2010;58(8):2905–2911. https://doi.org/10.1016/j.actamat.2010.01.019

Information about the Authors

Elena N. Korosteleva – Cand. Sci. (Eng.), Senior Research Scientist, Institute of Strength Physics and Materials Science of the Siberian Branch of the Russian Academy of Sciences (ISPMS SB RAS)
ORCID: 0000-0002-4363-3604
E-mail: elenak@ispms.ru

Anna G. Knyazeva – Dr. Sci. (Phys.-Math.), Professor, Chief Research Scientist, ISPMS SB RAS
ORCID: 0000-0002-9765-7695
E-mail: anna-knyazeva@mail.ru

Maria A. Anisimova – Cand. Sci. (Phys.-Math.), Junior Research Scientist, ISPMS SB RAS
ORCID: 0000-0002-5312-2496
E-mail: anmariia@ispms.ru

Ivan O. Nikolaev – Engineer, ISPMS SB RAS
ORCID: 0000-0003-4529-6477
E-mail: rmkast97@gmail.com

Сведения об авторах

Елена Николаевна Коростелева – к.т.н., ст. науч. сотрудник, Институт физики прочности и материаловедения Сибирского отделения РАН (ИФПМ СО РАН)
ORCID: 0000-0002-4363-3604
E-mail: elenak@ispms.ru

Анна Георгиевна Князева – д.ф.-м.н., проф., гл. науч. сотрудник ИФПМ СО РАН
ORCID: 0000-0002-9765-7695
E-mail: anna-knyazeva@mail.ru

Мария Александровна Анисимова – к.ф.-м.н., мл. науч. сотрудник ИФПМ СО РАН
ORCID: 0000-0002-5312-2496
E-mail: anmariia@ispms.ru

Иван Олегович Николаев – инженер ИФПМ СО РАН
ORCID: 0000-0003-4529-6477
E-mail: rmkast97@gmail.com

Contribution of the Authors

E. N. Korosteleva – goal and objectives of the study, conducting the experiments, analysis of the research results, correction of the text, formulation of the conclusions.
A. G. Knyazeva – model formulation, analytical solutions, analysis of the research results, writing the text, correction of the conclusions.
M. A. Anisimova – conducting the calculations, preparation of illustrations.
I. O. Nikolaev – preparation and management of the experiments, conducting the experiments.

Вклад авторов

Е. Н. Коростелева – постановка цели и задачи исследования, проведение экспериментов, анализ результатов исследований, корректировка текста, формулировка выводов.
А. Г. Князева – формулировка моделей, построение аналитических решений, анализ результатов исследований, подготовка текста статьи, корректировка выводов.
М. А. Анисимова – проведение расчетов, подготовка иллюстраций.
И. О. Николаев – подготовка эксперимента, проведение экспериментов.

Received 25.11.2022
Revised 02.12.2022
Accepted 05.12.2022

Статья поступила 25.11.2022 г.
Доработана 02.12.2022 г.
Принята к публикации 05.12.2022 г.